Journal of Materials Chemistry A

PAPER

Flexible CoO–graphene–carbon nanofiber mats as binder-free anodes for lithium-ion batteries with superior rate capacity and cyclic stability†

Cite this: J. Mater. Chem. A, 2014, 2, 5890

Ming Zhang,*[ab] Feilong Yan,[a] Xuan Tang,[a] Qiuhong Li,[a] Taihong Wang*[a] and Guozhong Cao*[b]

Received 19th January 2014
Accepted 28th January 2014

DOI: 10.1039/c4ta00311j

www.rsc.org/MaterialsA

Flexible mats composed of CoO–graphene–carbon nanofibers have been prepared by electrospinning and a subsequent thermal treatment. The flexible mats of CoO–graphene–carbon annealed at 650 °C exhibited discharge capacities of 760 and 690 mA h g^{-1} at the 252nd and 352nd cycle, respectively, at a current density of 500 mA g^{-1}, which are much higher than those of pure carbon, graphene–carbon, and CoO–carbon nanofibers at the respective cycles. The CoO–graphene–carbon nanofibers can deliver a discharge capacity of 400 mA h g^{-1} at a current density of 2 A g^{-1}, which is also higher than the values obtain for CoO–carbon and graphene–carbon nanofibers. The improved electrochemical properties of the flexible CoO–graphene–carbon nanofiber mats could be ascribed to the framework, which allows for fast diffusion of Li^+, the presence of graphene, which enhances the conductivity and the mechanical properties of the mats, and the defective sites that arise from the introduced CoO and graphene which can store Li^+. It is believed that the electrospinning method used to combine the material with graphene could be a useful approach to prepare flexible mats for lithium-ion batteries, supercapacitors, and fuel cells.

1 Introduction

Flexible devices are of great interest because of their potential for low-cost production, and have been investigated by various groups.[1,2] Developing flexible energy-storage equipment to meet the energy demands of flexible devices in of great significance.[3,4] Lithium-ion batteries (LIBs) are promising candidates in this area because of their intrinsic high energy density, relatively high power density, and environmental friendliness.[5–7] Accommodating frequent mechanical strain and still retaining high quality energy supply for long-time use is a very important aspect of flexible electrodes for LIBs. Currently, LIBs electrodes are, in general, non-flexible and still suffer from insufficient rate capacity, and inferior cyclic stability, especially for most anodes.[8–11] It is highly desirable to develop flexible electrodes with excellent properties for LIBs.

Carbon materials, especially graphene and carbon nanofibers, have been demonstrated in flexible electrodes for energy storage.[12,13] Carbon nanofibers with significant space within them have drawn greater attention because they are of more benefit for the fast diffusion of Li^+ than flexible graphene sheets.[8,9,14,15] However, their specific capacities are too low to satisfy the energy demands of humans because of their low theoretical capacity.[14] Modifying carbon materials with other materials of high theoretical capacity or introducing defective sites (or micropores) are both effective ways to improve their properties.[16–22] Recently, cobalt oxide compounds with different morphologies have been studied in the field of LIBs by many researchers owing to its relatively high specific capacity.[23–25] Cobalt compound–carbon nanofibers composites also have been a hot research topic in LIBs.[17,19,26,27] Unfortunately, carbon nanofibers may become fragile after cobalt oxide has been added in, resulting in brittle anodes.[28]

Graphene, a new type of 2-D carbon material, possesses excellent properties, including exceptional mechanical properties, high conductivity, and good stability.[29] Many studies on graphene-based composites have been published regarding energy storage applications.[30–34] For example, graphene can be used to improve the mechanical properties of nanofibers made by electrospinning.[35,36] Moreover, the graphene in these electrospun nanofibers could be employed as a conductive additive, enhancing the conductivity of the nanofibers and resulting in

[a]Key Laboratory for Micro-Nano Optoelectronic Devices of Ministry of Education, State Key Laboratory for Chemo/Biosensing and Chemometrics, Hunan University, Changsha, 410082, P.R. China. E-mail: zhangming@hnu.edu.cn; thwang@hnu.edu.cn

[b]Department of Materials Science & Engineering, University of Washington, Seattle, Washington, 98195, USA. E-mail: gzcao@uw.edu

† Electronic supplementary information (ESI) available: The diameter distribution of the nanofibers, EDS spectra of the CoO–G–C nanofiber mats (A650), fine XPS spectra for O 1s, N 1s, and C 1s of the CoO–G–C nanofibers (A650), TEM images of CoO–G–C (A650) and CoO–C (C650), TG curves of the CoO–G–C (A650) and CoO–C (C650) nanofibers, SEM images of the CoO–G–C samples annealed at different temperatures and a table summarizing the specific capacities and cycling properties of other CoO_x–carbon composites. See DOI: 10.1039/c4ta00311j

improved properties.[32,37] Nevertheless, preparing graphene-based nanofibers with excellent properties is not an easy task because the dispersion of graphene is poor in the solvents used for electrospinning.

In this study, flexible mats of CoO–graphene–carbon (CoO–G–C) nanofibers were synthesized by electrospinning followed by a careful thermal treatment. The graphene precursor was processed using a special method to improve its dispersion in the organic solvent used for electrospinning. Even though the content of graphene and CoO in the nanofibers was very low, the flexible mats exhibited a high specific capacity at a large current density, and excellent cyclic stability when used as binder-free anodes for LIBs. These research results demonstrated that there were many aspects to the effects that graphene had on the properties of the mats.

2 Experimental

2.1 Materials synthesis

Polyacrylonitrile (PAN, $M_w = 150\,000$, Sigma-Aldrich Co., Ltd., USA), cobalt(II) acetate tetrahydrate ($CoAc_2$, Alfa Aesar Co., Ltd., USA), and *N*,*N*-dimethylformamide (DMF, J. T. Baker Co., Ltd., USA) were used without any further purification. Graphene oxide (GO) was prepared according to the previous literature.[38,39] To enhance the dispersion of GO in DMF, the GO suspension was centrifuged and cleaned with DMF for several times. GO was then dispersed in DMF at a concentration of about 0.4 mg mL^{-1}. After this, the suspension was processed with ultrasonic waves for 30 min. To prepare the precursor solution for electrospinning, PAN, $CoAc_2$, and GO were dissolved in DMF, forming a solution in concentrations of 6.5 wt%, 2.5 wt% and 0.066 mg mL^{-1}, respectively. To prepare pure carbon fibers, a precursor without $CoAc_2$ and GO was also prepared. A precursor for nanofibers without graphene was prepared in a similar way except without GO. All of the precursor solution was transferred into a 3 mL springe with a stainless steel needle (with an inner diameter of 0.6 mm). A syringe pump controlled the flow rate of the precursor solution to about 0.3 mL h^{-1}. A piece of aluminum foil used as the collector was vertically positioned about 15 cm away from the needle. The needle was connected to a high voltage DC power supply to obtain a voltage of 13–17 kV. Under these conditions, pure PAN, PAN–GO, PAN–$CoAc_2$ and PAN–GO–$CoAc_2$ nanofibers were generated and formed mats. After being pre-oxidized at 225 °C in air for 6 h, the resulting brown films (PAN–GO–$CoAc_2$) were treated at 550–650 °C in nitrogen for 2 h in order to carbonize the PAN and/or decompose $CoAc_2$, and the product is denoted as CoO–G–C. The pure PAN, PAN–GO, and PAN–$CoAc_2$ nanofibers were treated in a similar way at 650 °C in order to obtain the corresponding samples. The final pure carbon, graphene–carbon and CoO–carbon (CoO–C) nanofibers are denoted as E650, F650, and C650, respectively.

2.2 Material characterization

The microstructures of the samples were characterized using a JEOL JSM-7000F scanning electron microscope (SEM), and a FEI Tecnai G2 F20 transmission electron microscope (TEM) operating at 200 kV accelerating voltage. The samples were also analyzed using X-ray photoelectron spectroscopy (XPS, Surface Science Instruments S-probe spectrometer). The binding energy scales were calibrated by assigning the lowest binding energy C1s peak (a binding energy of 285.0 eV). Elemental analysis of the samples was achieved using energy dispersive spectroscopy (EDS).

2.3 Electrochemical measurements

The mats (including the pure carbon, graphene–carbon, CoO–C, and CoO–G–C nanofibers) were directly used as binder-free anodes for electrochemical measurements aimed towards the storage of Li^+. A Celgard 2400 microporous polypropylene membrane was used as a separator to assemble coin cells (CR 2016). The electrolyte used was a solution of 1 M $LiPF_6$ in ethylene carbonate–dimethyl carbonate (1 : 1 by volume). Pieces of pure lithium foil were used as both the counter and reference electrodes. All of the cells were assembled in an argon-filled glove-box with the moisture and the oxygen levels less than 1 ppm. Discharge and charge measurements were carried out using an Arbin BT2000 and a LAND battery testing system with the cut off potentials being 0.01 V for discharge and 3 V for charge. All of the specific capacities in this study were calculated based on the weight of the mats. The cyclic voltammetry results were collected on a electrochemical workstation (CHI660B).

3 Results and discussion

3.1 Synthesis and characterization of CoO–G–C mats

Fig. 1a shows an SEM image of the as-prepared PAN–GO–$CoAc_2$ nanofibers. The noodle-like nanofibers have a diameter of about 220 nm and easily changed their position during the measurement, showing their low stability under electron beam bombardment and poor conductance. After treatment at 225 °C, the diameter of the nanofibers, without any obvious formation of nanoparticles, decreases to nearly 200 nm. Bright spots in the SEM images shown in Fig. 1a and b are due to the accumulation of charges and are an indication of the relatively poor conductance of the nanofibers. An SEM image of the CoO–G–C nanofibers is shown in Fig. 1c. The nanofibers, which have diameters of approximately 165 nm, are composed of dispersed nanoparticles and graphene in a carbon nanofiber matrix. Although the graphene is not directly observed in the SEM image, GO can be reduced to graphene using a thermal treatment.[40] The diameters of the CoO–G–C nanofibers decreased from 220 to 165 nm, which could be attributed to the decomposition of PAN and $CoAc_2$, as shown in Fig. S1.† As a comparison experiment, no GO was added and the final samples (CoO–C) are shown in Fig. 1d. The diameters of CoO–C nanofibers were approximately 175 nm. Furthermore, the nanoparticles on the CoO–C nanofibers were much less obvious than those on the CoO–G–C nanofibers. The pure carbon nanofibers (Fig. 1e) and graphene–carbon nanofibers (Fig. 1f) were similar to each other. The smaller diameters of the graphene–carbon

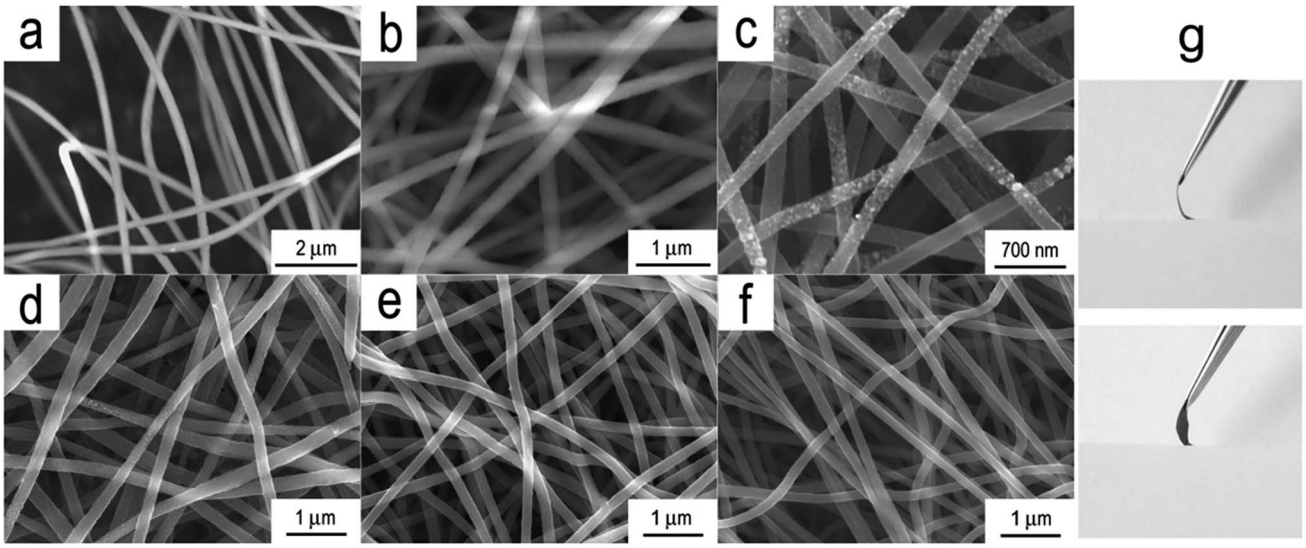

Fig. 1 SEM images of the as-prepared (a), treated at 225 °C (b), and annealed at 650 °C CoO–G–C nanofibers (c). SEM images of the nanofibers annealed at 650 °C: (d) CoO–C, (e) pure carbon, (f) graphene–carbon. Digital photos showing the flexibility of the CoO–G–C mats are displayed in (g).

nanofibers could be ascribed to the polarity of GO. Digital photos of the CoO–G–C mats are shown in Fig. 1g. A cross-sectional view of the mats (top) indicates that they are highly flexible. The photo taken from another angle (bottom) shows that there are no cracks in the mats, further demonstrating the flexibility of CoO–G–C.

TEM was used to characterize the micromorphology of the samples. Fig. 2a shows a TEM image of the CoO–G–C nanofibers. The nanofibers are about 165 nm in diameter, and the nanoparticles on the nanofibers are very small. Obviously, the distribution of nanoparticles is inhomogenous on the nanofibers in contrast to a previous report.[17] This phenomenon may be attributed to the oxygen-containing groups on GO affecting the nucleation and growth of the CoO nanoparticles. An magnified image is shown in Fig. 2b. The surface of the nanofibers is rough with an enlarged surface area and high porosity. Moreover, the nanoparticles are homogenously distributed in this magnified area. This special phenomenon could be attributed to graphene (although no graphene was observed) because of the effects that graphene has on the morphology of nanomaterials.[41] A high-resolution TEM image is shown in Fig. 2c. The nanoparticles are as small as approximately 5 nm. The *d*-spacing of the planes is 0.246 nm, which is very close to that of (111) plane for CoO (JCPDS 48-1719), implying that the nanoparticles are CoO. No graphene sheets are observed by TEM. A possible reason for this is that as the graphene sheets are in a low ratio in the composite they are covered up by carbon arising from PAN. Similar results can be found in the literature concerning graphene–carbon composites.[32,42] The microstructure of the CoO–G–C nanofibers is proposed based on the above result and shown schematically in Fig. 2d. The graphene could control the nucleation and growth of the CoO nanoparticles. The inhomogeneous distribution of graphene on the nanofibers results in the non-uniform dispersion of very small CoO nanoparticles, which is different to the CoO–C fibers without graphene.[17]

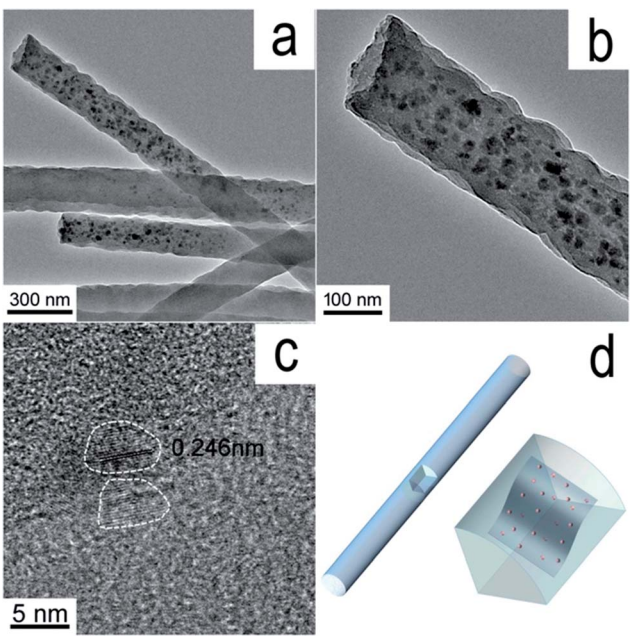

Fig. 2 (a–c) TEM images of CoO–G–C (A650) nanofibers at different magnifications. (d) A schematic diagram showing the inhomogeneous distribution of CoO nanoparticles on the CoO–G–C nanofibers.

XPS analysis was carried out on a Surface Science Instruments S-probe spectrometer in order to elucidate the bond state of the CoO–G–C samples prepared at 650 °C (marked as A650). Before measurement, this instrument was equipped with monochromatized Al K_α X-ray source and a low energy electron flood gun for charge neutralization of the non-conducting samples. The XPS spectrum of A650 shown in Fig. 3a exhibits four main peaks at about 285.0, 398.6, 531.5 and 780.4 eV, corresponding to the peaks of C 1s, N 1s, O 1s and Co 2p,

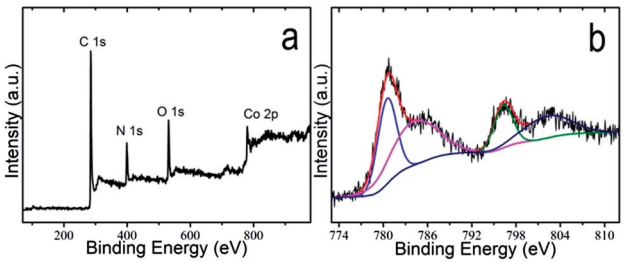

Fig. 3 (a) XPS spectra of the CoO–G–C nanofiber mats (A650) obtained at 650 °C. (b) The fine XPS spectrum of Co 2p indicates that the cobalt ions are Co^{2+}.

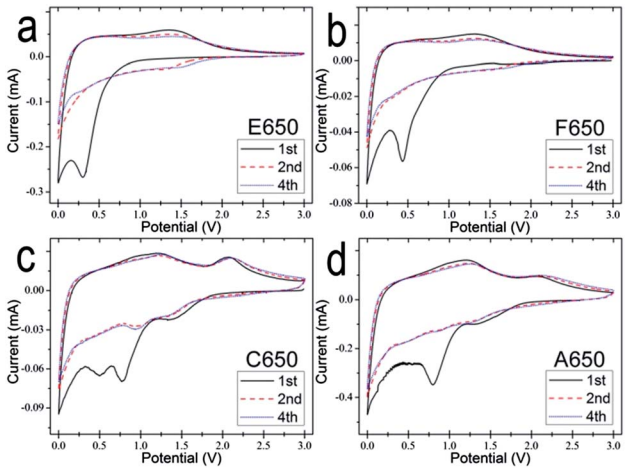

Fig. 4 CV curves of the pure carbon (E650, a), graphene–carbon (F650, b), CoO–C (C650, c), and CoO–G–C (A650, d) nanofiber samples at a scan rate of 0.3 mV s^{-1}.

respectively.[43–46] These results are highly consistent with those of EDS (as shown in Fig. S2†), in that there are four elements in each. The fine XPS spectrum of Co 2p in Fig. 3b exhibits two peaks at 780.4 and 796.2 eV associated with two satellite peaks, which are similar to those seen in previous reports about CoO.[43,44] The $2p_{3/2}$ peak at about 780.4 eV can be indexed to Co^{2+} coordinated to oxygen anions.[44] The satellite peak arising from the occurrence of a ligand-to-metal charge transfer during the photoemission process was used as a fingerprint for the recognition of high-spin Co(II) species in A650.[46] The above peak patterns and relative intensities of Co 2p matched well with the XPS spectra of well-characterized CoO standards in the literature, further demonstrating that these particles were CoO.[43,44,46] In Fig. S3a,† the peaks at 531.5 and 533.4 eV indicate the presence of oxygen-containing groups on the surface.[45,47] From another perspective, the O 1s peak at about 530 eV, which corresponds to oxygen species in the spinel cobalt oxide phase (Co_3O_4) is not observed, showing that the nanoparticles are CoO.[48] The fine XPS spectrum of N 1s is shown in Fig. S3b.† This shows the residual groups of PAN according to the raw materials. The N 1s peaks at 398.6 and 400.3 eV can be assigned to pyridine-type and conjugated nitrogen.[49] Both of the above nitrogen types have positive effects on the storage of Li^+, especially pyridine-type nitrogen.[50,51] The fine XPS spectrum of C 1s is shown in Fig. S3c.† The C 1s spectrum could be deconvoluted into five peaks, including peaks at 285 (graphitized carbon), 286.5 (carbon in phenolic and alcohol groups), 288 (carbon in carbonyl or quinine groups), 289.2 (carbon in carboxyl or ester groups), and 290.4 eV (carbon in adsorbed CO and CO_2). Similar results have been reported in a previous study concerning PAN-based carbon nanofibers,[52] indicating that there are some oxygen-containing groups in the nanofibers.

3.2 Electrochemical properties of CoO–G–C mats

CV measurements were carried out over a voltage range of 0–3 V to investigate the electrochemical mechanism, and the results are shown in Fig. 4. In Fig. 4a, the cathodic peak in the first cycle of E650 at about 0.4 V could be attributed to the irreversible formation of a solid electrolyte interface (SEI) film. There are two anodic peaks at about 0.2 (not obvious in the first cycle) and 1.3 V, which could be indexed to lithium extraction from graphite-like carbon and delithiation of the defective sites on the carbon nanofibers, respectively.[21,22,53] The CV curve of the second cycle nearly overlaps with the curve for the fourth cycle, showing the good cyclic stability of E650. The CV curves of F650 in Fig. 4b are similar to those of E650, showing that graphene has little effect on the electrochemical reactions of carbon. The CV curves of the C650 and A650 nanofibers are shown in Fig. 4c and d. During the first cycle, the cathodic peaks at about 1.35 V can be attributed to the electrochemical reduction of CoO with Li.[11,20] The peaks in the range of 0.5–0.9 V could be ascribed to the formation of SEI films.[20] The CV curves of both A650 and C650 show three anodic peaks at about 0.2, 1.25, and 2.1 V, which could be indexed to the delithiation of carbon, the extraction of Li from the defective sites, and the reformation of CoO, respectively.[9,20,54] The difference in the CV results between A650 and C650 is that the delithiation peak of CoO in C650 is more obvious than that of A650, which may be attributed to the smaller particle size of CoO in C650 (Fig. S4†). The anodic peaks (at about 1.25 V) of carbon in A650 and C650 are shifted to low potentials compared with pure carbon (E650), which could be attributed to the active effects of CoO on the carbon.[18] Furthermore, the anodic peaks for the delithiation of the defective sites at about 1.25 V for both A650 and C650 are stronger and broader than those of E650 and F650, indicating that more defective sites are introduced into the nanofibers due to the presence of CoO.[53] The almost overlapped CV curves of A650 and C650 in the 2^{nd} and 4^{th} cycles show good cyclic stability during the following cycles, demonstrating that graphene–carbon nanofibers are desirable frameworks for the anodes of LIBs. The difference between A650 and C650 is that the cathodic peak for the lithiation/delithiation of CoO in A650 is shifted to a lower potential and its anodic peak is shifted to a higher potential compared to the related peaks for CoO in C650, showing the larger particle size of CoO in A650, which is consistent with the TEM results (as shown in Fig. S4†).[55] A previous study also demonstrated that graphene oxide could affect the morphology and size of the nanoparticles.[41]

Therefore, the larger CoO nanoparticle size in A650 may be ascribed to the presence of graphene oxide in the precursor.

Fig. 5a shows a comparison of the discharge capacities of the samples (A650, C650, E650, and F650) as a function of the cycle number at different current densities. All of them show relatively good cyclic stability during the cycles. However, their discharge capacities at a current density of 0.1 A g^{-1} decrease from 1030 mA h g^{-1} (A650) to 520 mA h g^{-1} (E650). When the current density increases to 0.5 A g^{-1}, the corresponding discharge capacities decrease from 760 mA h g^{-1} (A650) to 395 mA h g^{-1} (C650) at the 252nd cycle. In addition, A650 could deliver a discharge capacity of 690 mA h g^{-1} at the 352nd cycle, showing superior cyclic stability and a high capacity. According to the TGA results (Fig. S5†), the mass ratio of CoO in both C650 and A650 is about 29.5%, showing less effects of graphene on the mass ratio of CoO in the nanofibers. A more interesting phenomenon is that the discharge capacity of A650 is much higher than both C650 and F650, demonstrating that the synergy between the three components (carbon, graphene, and CoO) is a critical factor in improving the electrochemical properties of the nanofiber mats. The discharge capacity of A650 is also higher than the theoretical specific capacity of CoO–G–C, which is calculated to be 533 mA h g^{-1} based on 29.5 wt% CoO and 70.5 wt% carbon (457 mA h g^{-1}, according to F650 after 252 cycles), which is more evidence of the synergistic effects in CoO–G–C. Comparing C650 with F650, it is clear that the discharge capacity of C650 is higher than that of F650 at a current density of 0.1 A g^{-1}, and it is inverted at a current of 0.5 A g^{-1}. This phenomenon demonstrates that CoO plays a key role in the improvement of the capacity, while the graphene has more influence on the enhancement of the rate capacity. Based on the results from the CV curves, the superior properties of A650 could be ascribed to the improved defective sites in A650. Comparing the properties of A650 with previous reports on CoO_x–C fibers arising from PAN,[17,19,26,27] it could be observed that the CoO–G–C mats (A650) demonstrated a relatively high specific capacity and superior cyclic stability, as shown in Table 1. Moreover, their properties are also better than some CoO_x–graphene and CoO_x–C composites with respect to the storage of Li^+ (as shown in Table S1†),[25,45,56–62] further indicating the advantages of using CoO–G–C mats as binder-free anodes for LIBs.

The effect of the annealing temperature on the properties of CoO–G–C was also investigated, and the results are shown in

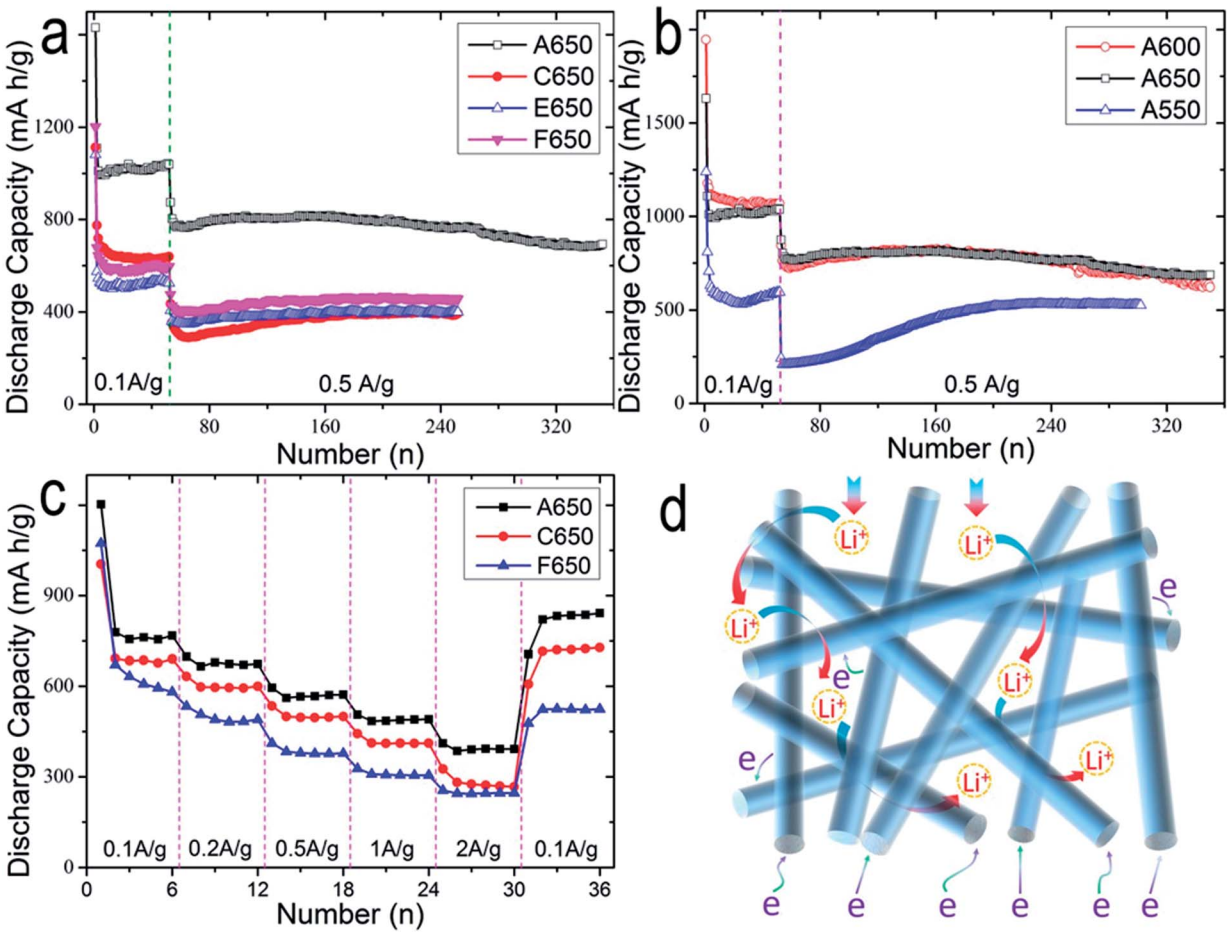

Fig. 5 (a) The cycling properties of the A650 (CoO–G–C), C650 (CoO–C), E650 (pure carbon), and F650 (graphene–carbon) samples. (b) Discharge capacity *vs.* cycle number curves of the A650, A600, and A550 samples. (c) The rate capacity of the A650, C650, and F650 samples. (d) A schematic diagram showing that the A650 nanofiber flexible mats are beneficial for the storage of Li^+.

Table 1 The specific capacities and cycling properties of the CoO_x–carbon composites as anodes for LIBs

	Capacity (mA h g^{-1})/current density (A g^{-1})			
Materials	50^{th}	100^{th}	Others	Ref.
Co–C fibers[a]	804/0.1			24
Co_3O_4–C fibers[a]	534/0.1 20^{th}			26
CoO–C fibers[a]	633/0.1 52^{nd}			27
CoO–C fibers[a]		853/0.14		17
Co_3O_4–CNT		530/0.09		25
CoO–graphene			640/0.1 150^{th}	56
CoO–C		725/0.2		57
CoO–C	700/0.1 70^{th}			58
Co_3O_4–graphene		732/0.15		59
CoO–graphene	1592/0.05			60
CoO–graphene	935/0.05			45
Co_3O_4–graphene		1005/0.074		61
Co_3O_4–CMK3	709/0.1 20^{th}			62
CoO–G–C mats[a]		800/0.5	690/0.5 352^{nd}	This study

[a] PAN-based fibers.

Fig. 5b. Although a high temperature (>700 °C) results in the carbon fibers with high conductance,[8] the CoO–G–C nanofibers are obtained at 550, 600, and 650 °C to avoid conversion of CoO to Co and the reduction of nitrogen. The samples are denoted as A550, A600, and A650, respectively. It can be observed from Fig. 5b that the capacities of A600 and A650 are much higher than that of A550, especially at a low current density. The inferior properties of A550 could be attributed the low degree of carbonization and poor conductance of the nanofibers. The properties of A650 are just a little better than those of A600, showing that the best annealing temperature for CoO–G–C is in the range of 600 to 650 °C. This result agrees with a recent study on PAN-based carbon for LIBs.[51] According to SEM images (Fig. S6†), the porosity of CoO–G–C improves from A550 to A650. Therefore, to achieve the best electrochemical properties of CoO–G–C, an optimal temperature is need that balances the porosity and the conductance of the nanofibers. To study the advanced property of the flexible CoO–G–C mats as anodes for LIBs, the rate capacity was evaluated, as shown in Fig. 5c. CoO–G–C (A650) maintains reversible capacities of 770, 680, 570, 490, and 400 mA h g^{-1} at current densities of 0.1, 0.2, 0.5, 1, and 2 A g^{-1}, respectively. These values are higher than those of CoO–C (C650) at the corresponding current densities. This improvement could be attributed to the enhanced conductance arising from graphene. The properties of CoO–G–C are also better than those of pure carbon (E650), showing the positive effects that the CoO nanoparticles have on the electrochemical properties of the nanofibers.

The above results have demonstrated that the flexible CoO–G–C mats showed improved properties with respect to the storage of Li^+. This improvement could be attributed to following reasons, based on their microstructure, as shown in Fig. 5d. Firstly, the CoO–G–C nanofiber mats with large pores are beneficial for the diffusion of Li^+.[63] Secondly, the mats of carbon fibers have a high conductance for the transfer of electrons, and decrease the polarization at a large current density. Thirdly, the graphene has good conductivity and could improve the conductance of the nanofibers.[37] Fourthly, the graphene can control the particle size of CoO and maintain the structural stability of the CoO nanoparticles.[31] Fifthly, the graphene has superior mechanical properties that could enhance the mechanical strength of the nanofibers and protect them from fracturing.[36] Sixthly, the flexible mats can accommodate large deformations without rupture. Seventhly, the flexible mats, when used as binder-free anodes for LIBs, could reduce the internal resistance of the battery and provide a high output voltage. Finally, CoO and graphene could introduce more defective sites into the carbon nanofiber mats, resulting in an improvement of the capacity for Li^+ storage.

4 Conclusions

Flexible mats of CoO–G–C nanofibers have been synthesized by electrospinning and a following thermal treatment. The results demonstrated that graphene could control the particle size of CoO during the synthesis procedure. When used as binder-free anodes for LIBs, the flexible mats made of CoO–G–C nanofibers showed improved cyclic stability along with a high specific capacity (690 mA h g^{-1} after 352 cycles at a current density of 500 mA g^{-1}) and an enhanced rate capacity (400 mA h g^{-1} at a current density of 2 A g^{-1}) compared with CoO–C, graphene–carbon, and pure carbon nanofiber mats. The improvement could be attributed to the framework of the mats, which allow the fast diffusion of Li^+, and the graphene, which has good mechanical properties and superior conductance that not only controls the particle size of CoO, but also improves the mechanical strength and conductivity of the flexible mats. In addition, the defective sites arising from the introduction of CoO and graphene can improve the storage of Li^+.

Acknowledgements

This research work has been financially supported in part by the National Science Foundation (NSF, CMMI-1030048), NESAC/BIO (EB-002027), and the University of Washington TGIF grant. Part of this work was conducted at the University of Washington NanoTech User Facility, a member of the NSF National Nanotechnology Infrastructure Network (NNIN). Ming Zhang would like to acknowledge the National Natural Science Foundation of China (61376073 and 21103046), the Hunan Provincial Natural Science Foundation of China (10JJ1011 and 11JJ7004), the China Scholarship Council and Fundamental Research Funds for the Central Universities.

Notes and references

1 X. Li, T. Gu and B. Wei, *Nano Lett.*, 2012, **12**, 6366–6371.
2 X. Jia, Z. Chen, A. Suwarnasarn, L. Rice, X. Wang, H. Sohn, Q. Zhang, B. M. Wu, F. Wei and Y. Lu, *Energy Environ. Sci.*, 2012, **5**, 6845–6849.

3 D. Kuang, J. r. m. Brillet, P. Chen, M. Takata, S. Uchida, H. Miura, K. Sumioka, S. M. Zakeeruddin and M. Grätzel, *ACS Nano*, 2008, **2**, 1113–1116.

4 F. Zhang, C. Yuan, J. Zhu, J. Wang, X. Zhang and X. W. Lou, *Adv. Funct. Mater.*, 2013, **23**, 3909–3915.

5 Y. Liu, M. Clark, Q. Zhang, D. Yu, D. Liu, J. Liu and G. Cao, *Adv. Energy Mater.*, 2011, **1**, 194–202.

6 J. Song, S. Chen, M. Zhou, T. Xu, D. Lv, M. L. Gordin, T. Long, M. Melnyk and D. Wang, *J. Mater. Chem. A*, 2014, **2**, 1257–1262.

7 D. Yu, C. Chen, S. Xie, Y. Liu, K. Park, X. Zhou, Q. Zhang, J. Li and G. Cao, *Energy Environ. Sci.*, 2011, **4**, 858–861.

8 J. K. Lee, K. W. An, J. B. Ju, B. W. Cho, W. I. Cho, D. Park and K. S. Yun, *Carbon*, 2001, **39**, 1299–1305.

9 L. W. Ji and X. W. Zhang, *Nanotechnology*, 2009, **20**, 155705.

10 W. Y. Li, L. N. Xu and J. Chen, *Adv. Funct. Mater.*, 2005, **15**, 851–857.

11 J. Jiang, J. Liu, R. Ding, X. Ji, Y. Hu, X. Li, A. Hu, F. Wu, Z. Zhu and X. Huang, *J. Phys. Chem. C*, 2009, **114**, 929–932.

12 V. Presser, L. Zhang, J. J. Niu, J. McDonough, C. Perez, H. Fong and Y. Gogotsi, *Adv. Energy Mater.*, 2011, **1**, 423–430.

13 S. Chen, J. Duan, Y. Tang and S. Zhang Qiao, *Chem. – Eur. J.*, 2013, **19**, 7118–7124.

14 C. Kim, K. S. Yang, M. Kojima, K. Yoshida, Y. J. Kim, Y. A. Kim and M. Endo, *Adv. Funct. Mater.*, 2006, **16**, 2393–2397.

15 B. Zhang, Y. Yu, Z. Huang, Y.-B. He, D. Jang, W.-S. Yoon, Y.-W. Mai, F. Kang and J.-K. Kim, *Energy Environ. Sci.*, 2012, **5**, 9895–9902.

16 M. Zhang, D. Lei, X. Yin, L. Chen, Q. Li, Y. Wang and T. Wang, *J. Mater. Chem.*, 2010, **20**, 5538–5543.

17 W.-H. Ryu, J. Shin, J.-W. Jung and I.-D. Kim, *J. Mater. Chem. A*, 2013, **1**, 3239–3243.

18 J. Yue, X. Zhao and D. Xia, *Electrochem. Commun.*, 2012, **18**, 44–47.

19 L. Wang, Y. Yu, P.-C. Chen and C.-H. Chen, *Scr. Mater.*, 2008, **58**, 405–408.

20 F. Li, Q.-Q. Zou and Y.-Y. Xia, *J. Power Sources*, 2008, **177**, 546–552.

21 N. Takami, A. Satoh, M. Oguchi, H. Sasaki and T. Ohsaki, *J. Power Sources*, 1997, **68**, 283–286.

22 Y.-P. Wu, C.-R. Wan, C.-Y. Jiang, S.-B. Fang and Y.-Y. Jiang, *Carbon*, 1999, **37**, 1901–1908.

23 J.-S. Do and C.-H. Weng, *J. Power Sources*, 2005, **146**, 482–486.

24 Y. Ding, P. Zhang, Z. Long, Y. Jiang, J. Huang, W. Yan and G. Liu, *Mater. Lett.*, 2008, **62**, 3410–3412.

25 G. Wang, X. Shen, J. Yao, D. Wexler and J.-H. Ahn, *Electrochem. Commun.*, 2009, **11**, 546–549.

26 P. Zhang, Z. P. Guo, Y. Huang, D. Jia and H. K. Liu, *J. Power Sources*, 2011, **196**, 6987–6991.

27 M. Zhang, E. Uchaker, S. Hu, Q. Zhang, T. Wang, G. Cao and J. Li, *Nanoscale*, 2013, **5**, 12342–12349.

28 L. Wang, Y. Yu, P. C. Chen, D. W. Zhang and C. H. Chen, *J. Power Sources*, 2008, **183**, 717–723.

29 M. J. Allen, V. C. Tung and R. B. Kaner, *Chem. Rev.*, 2010, **110**, 132–145.

30 M. Zhang, B. Qu, D. Lei, Y. Chen, X. Yu, L. Chen, Q. Li, Y. Wang and T. Wang, *J. Mater. Chem.*, 2012, **22**, 3868–3874.

31 C. H. Kim, B.-H. Kim and K. S. Yang, *Carbon*, 2012, **50**, 2472–2481.

32 Z. Tai, X. Yan, J. Lang and Q. Xue, *J. Power Sources*, 2012, **199**, 373–378.

33 J. Liang, Y. Jiao, M. Jaroniec and S. Z. Qiao, *Angew. Chem., Int. Ed.*, 2012, **51**, 11496–11500.

34 B. Das, B. Choudhury, A. Gomathi, A. K. Manna, S. K. Pati and C. N. R. Rao, *ChemPhysChem*, 2011, **12**, 937–943.

35 Q. Bao, H. Zhang, J.-x. Yang, S. Wang, D. Y. Tang, R. Jose, S. Ramakrishna, C. T. Lim and K. P. Loh, *Adv. Funct. Mater.*, 2010, **20**, 782–791.

36 Y. He, N. Zhang, Q. Gong, H. Qiu, W. Wang, Y. Liu and J. Gao, *Carbohydr. Polym.*, 2012, **88**, 1100–1108.

37 N. Zhu, W. Liu, M. Xue, Z. Xie, D. Zhao, M. Zhang, J. Chen and T. Cao, *Electrochim. Acta*, 2010, **55**, 5813–5818.

38 W. S. Hummers and R. E. Offeman, *J. Am. Chem. Soc.*, 1958, **80**, 1339.

39 M. Zhang, D. Lei, Z. Du, X. Yin, L. Chen, Q. Li, Y. Wang and T. Wang, *J. Mater. Chem.*, 2011, **21**, 1673–1676.

40 Z.-S. Wu, W. Ren, L. Gao, J. Zhao, Z. Chen, B. Liu, D. Tang, B. Yu, C. Jiang and H.-M. Cheng, *ACS Nano*, 2009, **3**, 411–417.

41 H. Wang, H. S. Casalongue, Y. Liang and H. Dai, *J. Am. Chem. Soc.*, 2010, **132**, 7472–7477.

42 S. Yi, J. Chen, H. Li, L. Liu, X. Xiao and X. Zhang, *Carbon*, 2010, **48**, 926–928.

43 C. V. Schenck, J. G. Dillard and J. W. Murray, *J. Colloid Interface Sci.*, 1983, **95**, 398–409.

44 R. Dedryvère, S. Laruelle, S. Grugeon, P. Poizot, D. Gonbeau and J. M. Tarascon, *Chem. Mater.*, 2004, **16**, 1056–1061.

45 Z.-S. Wu, W. Ren, L. Wen, L. Gao, J. Zhao, Z. Chen, G. Zhou, F. Li and H.-M. Cheng, *ACS Nano*, 2010, **4**, 3187–3194.

46 D. Barreca, C. Massignan, S. Daolio, M. Fabrizio, C. Piccirillo, L. Armelao and E. Tondello, *Chem. Mater.*, 2001, **13**, 588–593.

47 L. Fu, Z. Liu, Y. Liu, B. Han, P. Hu, L. Cao and D. Zhu, *Adv. Mater.*, 2005, **17**, 217–221.

48 B. Varghese, C. H. Teo, Y. Zhu, M. V. Reddy, B. V. R. Chowdari, A. T. S. Wee, V. B. C. Tan, C. T. Lim and C. H. Sow, *Adv. Funct. Mater.*, 2007, **17**, 1932–1939.

49 Y. Wu, S. Fang and Y. Jiang, *Solid State Ionics*, 1999, **120**, 117–123.

50 Y. P. Wu, C. Y. Jiang, C. R. Wan, S. B. Fang and Y. Y. Jiang, *J. Appl. Polym. Sci.*, 2000, **77**, 1735–1741.

51 B. Zhang, Y. Yu, Z.-L. Xu, S. Abouali, M. Akbari, Y.-B. He, F. Kang and J.-K. Kim, *Adv. Energy Mater.*, 2013, DOI: 10.1002/aenm.201301448.

52 J.-H. Zhou, Z.-J. Sui, J. Zhu, P. Li, D. Chen, Y.-C. Dai and W.-K. Yuan, *Carbon*, 2007, **45**, 785–796.

53 B. Guo, X. Wang, P. F. Fulvio, M. Chi, S. M. Mahurin, X.-G. Sun and S. Dai, *Adv. Mater.*, 2011, **23**, 4661–4666.

54 C. F. Zhang, X. Peng, Z. P. Guo, C. B. Cai, Z. X. Chen, D. Wexler, S. Li and H. K. Liu, *Carbon*, 2012, **50**, 1897–1903.
55 C.-H. Lu and S.-W. Lin, *J. Power Sources*, 2001, **97–98**, 458–460.
56 X.-L. Huang, R.-Z. Wang, D. Xu, Z.-L. Wang, H.-G. Wang, J.-J. Xu, Z. Wu, Q.-C. Liu, Y. Zhang and X.-B. Zhang, *Adv. Funct. Mater.*, 2013, **23**, 4345–4353.
57 W. Yao, J. Chen and H. Cheng, *J. Solid State Electrochem.*, 2011, **15**, 183–188.
58 S. Xiong, J. S. Chen, X. W. Lou and H. C. Zeng, *Adv. Funct. Mater.*, 2012, **22**, 861–871.
59 J. Zhu, Y. K. Sharma, Z. Zeng, X. Zhang, M. Srinivasan, S. Mhaisalkar, H. Zhang, H. H. Hng and Q. Yan, *J. Phys. Chem. C*, 2011, **115**, 8400–8406.
60 C. Peng, B. Chen, Y. Qin, S. Yang, C. Li, Y. Zuo, S. Liu and J. Yang, *ACS Nano*, 2012, **6**, 1074–1081.
61 G. Wang, J. Liu, S. Tang, H. Li and D. Cao, *J. Solid State Electrochem.*, 2011, **15**, 2587–2592.
62 H. Zhang, H. Tao, Y. Jiang, Z. Jiao, M. Wu and B. Zhao, *J. Power Sources*, 2010, **195**, 2950–2955.
63 H.-X. Zhang, C. Feng, Y.-C. Zhai, K.-L. Jiang, Q.-Q. Li and S.-S. Fan, *Adv. Mater.*, 2009, **21**, 2299–2304.